Structural properties of epitaxial α-U thin films on Ti, Zr, W and Nb

R. Nicholls [1,*] D. A. Chaney [2] G. H. Lander,[1] R. Springell,[1] and C. Bell[1]
[1]*H. H. Wills Physics Laboratory, University of Bristol, Bristol BS8 1TL, United Kingdom*
[2]*European Synchrotron Radiation Facility, 71 avenue des Martyrs, 38000 Grenoble, France*

(Received 8 August 2023; accepted 21 November 2023; published 15 December 2023)

Thin layers of orthorhombic uranium (α-U) have been grown onto buffered sapphire substrates by dc magnetron sputtering, resulting in the discovery of new epitaxial matches to Ti(00.1) and Zr(00.1) surfaces. These systems have been characterized by x-ray diffraction and reflectivity and the optimal deposition temperatures have been determined. More advanced structural characterization of the known Nb(110) and W(110) buffered α-U systems has also been carried out, showing that past reports of the domain structures of the U layers are incomplete. The ability of this low symmetry structure to form crystalline matches across a range of crystallographic templates highlights the complexity of U metal epitaxy and points naturally toward studies of the low temperature electronic properties of α-U as a function of epitaxial strain.

DOI: 10.1103/PhysRevMaterials.7.123602

I. INTRODUCTION

Many of the actinides and their compounds exhibit fascinating condensed matter physics, including a plethora of unusual structural and electronic ground states (e.g., complex polymorphism, unconventional magnetic ordering, and heavy fermion superconductivity). These properties often arise as a result of the outer-shell $5f$ electrons being situated on the boundary between itinerancy and localization [1–5]. The midseries actinide metals (U, Np, Pu) exemplify these characteristics, with each of the three distinct crystallographic structures adopted by bulk U exhibiting notable collective electronic phenomena at low temperatures [6,7].

The thermodynamically stable phase of uranium under ambient conditions is orthorhombic α-U ($Cmcm$). This phase is unique amongst the elements, both for its low symmetry crystal structure and for its unusual electronic properties, with bulk α-U crystals undergoing a series of three charge density wave (CDW) transitions before entering a superconducting (SC) state. Although the superconducting transition temperature (T_c) appears to vary unpredictably with sample crystallinity and purity ($T_c = 0.02$–0.78 K), it is generally accepted that isotropic compressive pressure can be used to suppress the CDW transitions and enhance T_c to a maximum of 2 K near 1.5 GPa [8–10]. The exact nature of the interaction between the SC and CDW states in α-U is yet to be understood, but a combination of bulk and thin film studies have since confirmed that pressure-induced changes to the low temperature states are related primarily to the length of the a axis [11,12].

Epitaxial strain engineering can often be used to explore regions of phase space that are inaccessible in bulk experiments involving uranium. For example, epitaxial layers of α-U with $a_{\text{film}} \approx a_{\text{bulk}}$ host an incommensurate "bulklike" CDW below 43 K, while U layers with $a_{\text{film}} > a_{\text{bulk}}$ (i.e., a strain that would be difficult to attain in bulk crystals) host a near-commensurate CDW with an increased onset temperature of 120 K [12,13]. Compression of the c axis and expansion of the b axis are both predicted to stabilize the CDW state in α-U [14], but the influence of uniaxial strain along these axes has not yet been explored.

It is also known that deposition onto other crystallographic templates can produce well-ordered overlayers that are difficult to stabilize in the bulk. Recently, crystalline layers of the tetragonal β-U phase have been stabilized at room temperature via deposition onto Si(111) [15] and single crystal layers of a pseudo-body-centered-cubic γ-U structure have been realized by the codeposition of U and Mo onto Nb(110) [16]. Uranium may also form a "hexagonal-close-packed" (hcp) structure that is not found in the bulk when deposited on W(110) [17–19], Gd(00.1) [13,20], and Cu(111) or Ir(111) buffer layers, although the U layers in the final two systems gradually transition back into α-U [21].

Given the rich array of nearly degenerate structural ground states, it is often difficult to predict the phase and orientation that a uranium layer will form under specific growth conditions. A key task in this area is, therefore, to examine a range of metallic buffer layers that can be used to stabilize high quality epitaxial layers of each U allotrope. The range of strains, structures, and orientations will allow further exploration of their intriguing electronic properties, provided the complex crystallographic domain structures are also fully characterized. In this work we investigate the epitaxy of α-U onto two new buffer layers (Ti, Zr) and revisit the Nb and W systems from Ref. [22] to add new information to the previously reported domain structures.

Section II of this paper describes the growth and characterization procedures for each thin film system. Section III

*beckie.nicholls@bristol.ac.uk

TABLE I. Growth temperatures (T) and nominal layer thicknesses (t) for α-U thin films (subscript "U") deposited onto various buffer layers (subscript "B") and substrates. Layers grown without any intentional substrate heating are denoted as 20 °C. Each sample has been capped with a passivating layer (thickness t_C), deposited at room temperature. Typical room temperature deposition rates for each element were 0.38 (Ti), 0.70 (Zr) 0.35 (Nb), 0.48 (Ir), 0.44 (W) and 1.2–1.4 Å/s (U).

Substrate	Buffer	T_B (°C)	t_B (Å)	T_U (°C)	t_U (Å)	Cap	t_C (Å)
Al_2O_3(11.0)	Nb(110)	800	200	600	5000	Nb	130
Al_2O_3(11.0)	W(110)	750	85	450	1000	W	90
Al_2O_3(00.1)	Zr(00.1)	700	220	20, 250, 400, 500	520	Nb	150
Al_2O_3(00.1)	Ti(00.1)	600	180	20, 200, 400, 600	600	Ir or Ti	85 or 180

explores the structure and orientation of crystalline α-U grown onto Ti, Zr and W buffers as discerned from laboratory-based x-ray diffraction (XRD) and x-ray reflectivity (XRR). The epitaxy and interface quality in the Ti/U and Zr/U systems are explored as a function of temperature using these techniques. Also included in Sec. III are synchrotron x-ray diffraction measurements of epitaxial Nb/α-U(110) systems which reveal a previously unreported domain. The physical origin of the domain is discussed.

II. EXPERIMENTAL METHODS

A. Growth of epitaxial α-U films

All samples in this study were grown using the actinide dc magnetron sputtering system at the University of Bristol, UK. This ultrahigh vacuum system operates at base pressures of the order 10^{-10} mbar and contains four sputtering guns inside a load-locked chamber [23]. Substrates are loaded onto an adjustable height stage adjacent to a resistive heater capable of achieving temperatures of up to 850 °C. The substrates for epitaxial Ti(00.1) and Zr(00.1) growth were c-plane Al_2O_3(00.1) and the substrates for Nb(110) and W(110) growth were a-plane Al_2O_3(11.0). All substrates (sourced from MTI Corp) were polished to optical grade.

The nominal layer thicknesses and growth temperatures are given in Table I. The buffer growth temperature is denoted as T_B and the uranium growth temperature as T_U with respective film thicknesses t_B and t_U. Each sample was capped with a layer of a corrosion resistant metal deposited at room temperature in order to protect the U from *ex situ* oxidation. All layers were deposited using approximately 7.5×10^{-3} mbar high purity argon gas as the sputtering medium.

B. Structural characterization

Structural characterization of the Ti/U, Zr/U and W/U systems was performed using a Philips X'Pert diffractometer with a Cu K_α source. XRR profiles were modeled using the GENX package, where the error bars on each fitting parameter are calculated from a 5% change in the optimal figure of merit [24]. Characterization of the Nb/U system was performed using the diffuse scattering diffractometer at the ID28 beamline (ESRF, France) [25]. Synchrotron data were treated using the CRYSALIS PRO software package [26]; high resolution reciprocal space maps were produced using in-house programs and visualized in the DECTRIS ALBULA package [27]. All x-ray measurements were conducted at room temperature.

III. RESULTS AND DISCUSSION

A. Titanium buffered system

Titanium was sputtered onto Al_2O_3(00.1) substrates at 600 °C to produce epitaxial hexagonal-close-packed Ti(00.1) layers with the in-plane relationship $[10.0]_{Ti} \parallel [1\bar{1}.0]_{Al_2O_3}$ and thickness 180 Å. Uranium layers with a nominal thickness of 520 Å were subsequently deposited at various temperatures. Figure 1 shows the coupled 2θ-ω scans and rocking curves from the temperature series. XRR profiles with discernible Kiessig fringes are included as Supplemental Material [28]. Table II summarizes the d_{110} spacings, widths of each rocking curve ($\Delta\omega$), and the XRR-derived root-mean-square roughnesses (σ) across the series.

At the two lowest tested deposition temperatures, the U layer forms crystalline α-U(110). At $T_U = 20$ °C, the out-of-plane spacing ($d_{110} = 2.578$ Å) is 0.44% larger than bulk ($d_{110} = 2.567$ Å) and the peak asymmetry suggests a strain gradient from smaller to larger d_{110} spacings across the vertical extent of the film. Least-squares refinement from the positions of multiple off-specular reflections gives $a = 2.862$ Å (+0.26%), $b = 5.943$ Å (+1.34%), $c = 4.988$ Å (+0.67%), and an atomic cell volume of $V = 21.207$ Å^3 (+2.3%), where all percentages given are relative to bulk U at room temperature from Ref. [29].

At $T_U = 200$ °C, the specular α-U(110) peak is instead symmetric and close to the bulk value, with lattice parameters of $a = 2.858$ Å (+0.14%), $b = 5.854$ Å (−0.25%), $c = 4.993$ Å (+0.76%), and an atomic volume of $V = 20.885$ Å^3 (+0.65%) indicating that the b-axis strain has changed from tensile to compressive while the c-axis expansion persists. The Laue fringes are suggestive of high crystallinity and a sharp U-Ti interface. The periodicity of the oscillations can be used to extract the crystalline ordered volume, with the agreement between $t_{Laue} = 500 \pm 10$ Å and the XRR derived thickness of $t_U = 514 \pm 6$ Å suggesting that crystalline order is maintained throughout the full thickness of the U layer. The rocking curve also adopts the distinctive two-component line shape common to many high quality thin films [30,31].

The in-plane epitaxial relationships in these two well-ordered systems were determined from the in-plane (ϕ) dependence of the Ti(10.3) and U(221) off-specular reflections. The example data set shown in the top panel of Fig. 2 indicates an approximate alignment of

$$(00.1)_{Ti} \parallel (110)_U, \quad [01.0]_{Ti} \parallel [1\bar{1}0]_U.$$

The epitaxy is likely to be governed by the match shown in the bottom panel of Fig. 2 where the misfit strain $(d_U - d_{Ti})/d_{Ti}$ at

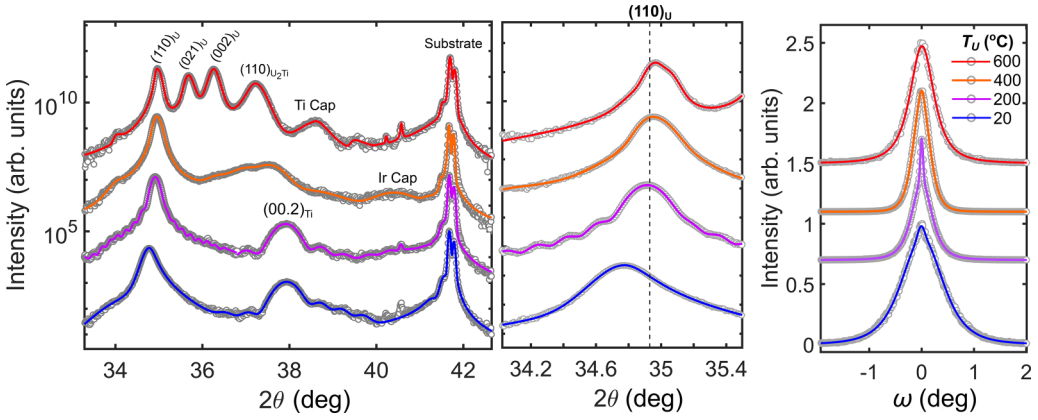

FIG. 1. Left: specular XRD (2θ-ω) scans of layers of U deposited onto Ti(00.1) buffers at various temperatures shown on a logarithmic scale to highlight the Laue fringes. The system transitions from pure, strained α-U(110) into a mixture of elemental metals and intermetallic compounds as T_U increases. Center: detail around $2\theta = 35°$ showing a systematic shift of the U(110) peak position with T_U. Vertical dashed line shows the bulk 2θ position. Right: evolution of the α-U(110) rocking curve. In all cases, data sets are offset vertically for clarity and solid lines are fits to the data.

room temperature is −3.2%. As hcp-Ti is sixfold symmetric in the (00.1) plane, any $60n°$ ($n \in Z$) in-plane rotation of the U layer brings the relevant planes into alignment. This should result in six energetically equivalent ways for the first monolayer of uranium to nucleate on the Ti(00.1) surface, as confirmed by the 60° separation of the $(221)_U$ peaks in the ϕ scan.

The stability of epitaxial α-U at these relatively low deposition temperatures was unexpected, as epitaxial Nb(110)/α-U(110) and W(110)/α-U(001) systems are typically grown at 450–600 °C [12,13,22]. In the case of Ti/U, temperatures above 200 °C are clearly detrimental to the quality of the interface. The degradation of the XRR signal, rocking curve profile, and U/Ti Laue fringes all suggest that the sharp U-Ti interface, and hence the coherent epitaxial match, has been partially lost at $T_U = 400$ °C and fully lost at $T_U = 600$ °C. The additional, nonelemental diffraction peaks seen in the 2θ-ω scans are likely to originate from Ti-rich alloys ($2\theta = 36$–$38°$) and U_2Ti ($2\theta_{110} = 37.2°$) [32].

B. Zirconium buffered system

A similar series was grown using zirconium buffer layers deposited onto c-plane sapphire at 700 °C. These single crystal Zr(00.1) layers adopt an in-plane epitaxial relationship of $Al_2O_3[10.0] \parallel Zr[10.0]$ and exhibit rocking curves with widths of 1–2°. This limits the mosaic spread and grain size of subsequent U layers, but the epitaxial relationships are still of interest. Figure 3 shows the coupled 2θ-ω scans for the series.

At room temperature, the spectrum is primarily α-U(110) with small inclusions of α-U(001). The off-specular

TABLE II. Parameters extracted from XRD/XRR measurements for the Ti/U temperature series. Values are not provided in cases where U-Ti intermixing has destroyed the coherent Ti buffer. The rocking curve width ($\Delta\omega$) represents the full width at half maximum (FWHM) of the broadest component in the peak profile; samples *underlined* also contain a resolution-limited Gaussian (see main text for details). Root-mean-square roughness (σ) values were extracted from GenX models fitted to XRR data.

T_U (°C)	d_{110} (Å)	$\Delta\omega_U$ (deg)	V_{XRD} (Å^3)	σ_U (Å)
20	2.578	0.933	21.207	16 ± 3
200	2.568	0.455	20.885	14 ± 3
400	2.565	0.370		
600	2.564	0.543		

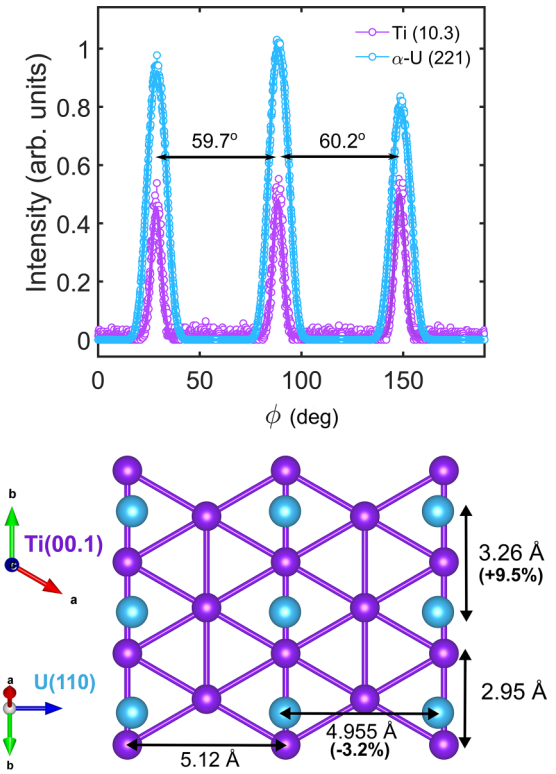

FIG. 2. Top: angular dependence of the off-specular reflections in an epitaxial Ti(00.1)/α-U(110) sample deposited at 200 °C. Bottom: two-dimensional illustration of the expected epitaxial match for a single U domain, showing the alignment of $d_U = c_U = 4.955$ Å and $d_{Ti} = 2d_{100} = 5.12$ Å. All quoted lattice parameters are bulk experimental values at room temperature from literature.

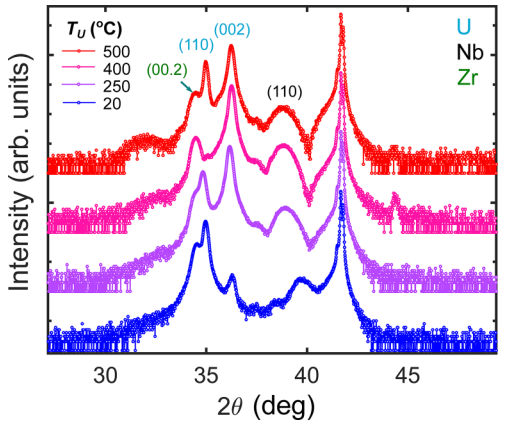

FIG. 3. 2θ-ω scans of U layers deposited onto Zr(00.1) buffer layers at various temperatures. Elemental U and Zr peaks are present across the entire temperature range, but the dominant U orientation varies with deposition temperature. Data are offset vertically and presented on a logarithmic intensity scale for clarity.

reflections, included as Supplemental Material [28], suggest an orientation relationship of

$$(00.1)_{Zr} \parallel (110)_U, \quad [10.0]_{Zr} \parallel [1\bar{1}0]_U,$$

where the alignment of $d_U = \frac{1}{2}(a_U^2 + b_U^2) = 3.26$ Å and $a_{Zr} = 3.24$ Å produces a low misfit strain of -0.6%. As with the Ti/α-U(110) system, the hexagonal symmetry of the buffer facilitates six equivalent matches in 360°. The measured α-U lattice parameters are $a = 2.853$ Å (-0.015%), $b = 5.826$ Å (-0.73%), and $c = 5.136$ Å ($+3.6\%$) and the atomic volume of $V = 21.346$ Å^3 ($+3.1\%$) is unusually large, even for a structure as malleable as α-U.

As the deposition temperature is increased toward 400 °C, the sample gradually becomes pure α-U(001), with the $(002)_U$ reflection gaining relatively weak Laue fringes. The orientation relationship between the layers determined from the Zr(10.5) and α-U(023) reflections (Fig. S3 in the Supplemental Material [28]) is

$$(00.1)_{Zr} \parallel (001)_U, \quad [10.0]_{Zr} \parallel [100]_U,$$

where the alignment of $d_U = 5.869$ Å and $d_{Zr} = 5.61$ Å results in a large misfit strain of $+4.6\%$. The refined lattice parameters are $a = 2.865$ Å ($+0.39\%$), $b = 5.827$ Å (-0.71%), and $c = 4.952$ Å (-0.05%) and the atomic volume is bulklike at $V = 20.67$ Å^3. Again, sixfold symmetry is seen in the α-U(023) ϕ scan due to the six equivalent matches with the hexagonal Zr(00.1) surface.

The transition from an α-U(110) layer with a low strain epitaxial match and a large atomic volume to an α-U(001) layer with a large misfit strain and a bulklike atomic volume suggests it is energetically favorable for the α-U structure to revert to a bulklike atomic volume at the expense of the epitaxial match and quality of the interface. The formation of an interfacial U-Zr layer that may influence the epitaxy is also suggested by the data.

A 1–2 nm reduction in t_U with increasing T_U is seen via the XRR-derived U layer thicknesses and, at 500 °C, the reflectivity profile no longer shows Kiessig fringes. A gradual reduction in the intensity of the $(00.2)_{Zr}$ reflection with

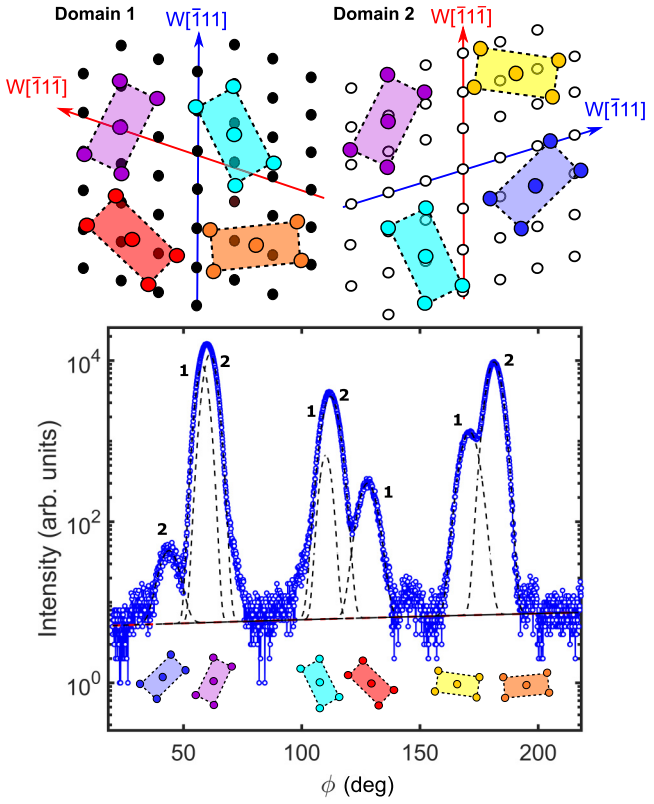

FIG. 4. Top: expected epitaxial matches for α-U(001) deposited onto a twinned W(110) buffer layer, adapted from [22]. Tungsten domains 1 and 2 represented by filled and open circles. Colors used to represent "unique" uranium domains. Each vertical tungsten axis is aligned with Al_2O_3[00.1]. Bottom: new ϕ scan of the off-specular U(023) reflection in a new α-U(001) system. Each peak has been matched to the relevant colored domains (colored images below) and individual fitted peak components (black dotted lines) are ascribed to the relevant W domain, with labels 1 and 2, respectively.

increasing T_U also suggests the formation of an interfacial U-Zr layer that increases in thickness with T_U. The strains generated by the unusually large mismatch between the Zr(00.1) and α-U(001) layer ($+4.6\%$) may be relieved by such a transition region, facilitating the observed change in orientation and reduction in atomic volume.

C. Tungsten buffered systems

The growth of complex, multidomain α-U(001) was first reported in 2008 [22]. Ward *et al.* proposed a model wherein eight domains of α-U nucleate on a twinned W(110) buffer as a result of a close match between the distances $d_U = 2.556$ Å (d_{110}) and $d_W = 2.584$ Å ($2d_{112}$). The two W domains and eight U domains are illustrated in the top panel of Fig. 4. In this idealized system, certain U domains (shown here in light blue and purple) are "degenerate" with respect to the buffer and so a total of six peaks should be resolvable using a point detector and in-plane ϕ scans. However, only four domains were seen in the original study [22].

The bottom panel of Fig. 4 shows a ϕ scan of the α-U(023) reflections in a new, high quality W/U sample. This scan maps

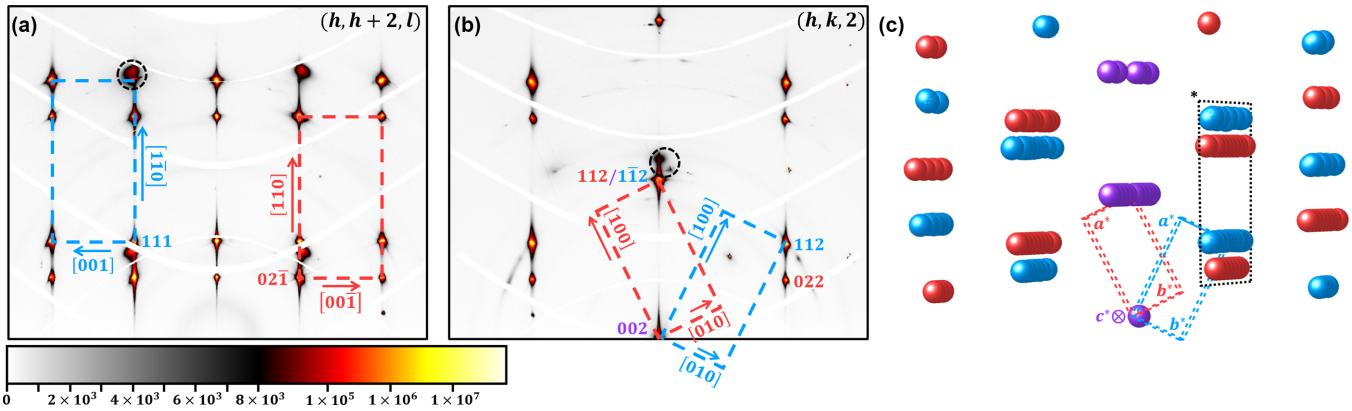

FIG. 5. RSMs for (a) the $(h, h+2, l)$ and (b) the $(h, k, 2)$ type planes reconstructed and denoted within the primary domain setting. Scale is linear white-black and $\log_{10}$ black-red-white. Single reciprocal space net units for the primary (red) and secondary (blue) domains are shown by dashed lines with select reflections indexed. Examples of sharp sapphire reflections and weak, broad Nb buffer reflections are highlighted within black dashed circles. (c) 3D reciprocal space schematic showing a selection of indexed reflections. Sphere color corresponds to domain origin consistent with left-hand panels. Degenerate reflections in the "specular plane" indicated by purple spheres. Reciprocal unit cells are shown as dashed cuboids with reciprocal lattice vectors marked. A section of the $(h, h+2, l)$ type plane shown in panel (a) is highlighted by a dashed black box and asterisk.

the relative orientations of any (010) planes (i.e., the b axes) in the α-U(001) layer. The scan shows six well-resolved peaks at angular separations that correlate well with the matches predicted by Ward *et al.* A total of *eight* peaks are required for an accurate fit as there is a slight misorientation between the reflections from the two degenerate (light blue and purple) pairs of domains, presumably due to strains in the buffer. These strains are also likely to be the cause of the unequal peak intensities, which imply there are strong preferences for certain U orientations. The crystalline quality of the U layer is significantly improved by reducing the deposition temperature to 450 °C used in Ref. [12] as opposed to 600 °C used in Ref. [22].

D. Niobium buffered systems

To date, all epitaxial films of α-U(110) on Nb(110) have been reported as single domain systems where the epitaxy is governed by a unidirectional in-plane match between $d_U = \frac{1}{2}(a_U^2 + b_U^2)^{\frac{1}{2}} = 3.264$ Å and $a_{Nb} = 3.311$ Å [13,22]. New reciprocal space maps (RSMs) taken at the ID28 beamline (ESRF) reveal a second domain consistently missed by point-detector measurements. These domains are referred to as primary "red" and secondary "blue" in the following discussions.

This unusual situation has arisen as the (hhl) reflections—i.e., those commonly used to check the symmetry of the U layer in laboratory ϕ scans—are coincident, but the degeneracy is clearly lifted outside of this plane. The $(h, h{+}2, l)$ RSM in Fig. 5(a) shows an example of a fully nondegenerate plane of reflections in a Nb(110)/U system, while the $(h, k, 2)$ type RSM in Fig. 5(b) demonstrates both the coincidence of reflections in the (hhl) plane and splitting away from this plane. Figure 5(c) shows the location in reciprocal space for a selection of the observed reflections, where the overlapping reflections from the two distinct domains (red and blue) are represented by purple spheres. The two α-U domains are related by an approximately 52° clockwise rotation about a shared $\boldsymbol{c}^*$ axis set into the page, where the experimentally determined reciprocal space transformation matrix

$$\frac{1}{4010}\begin{bmatrix} 2451 & 1549 & 0 \\ -6461 & 2461 & 0 \\ 0 & 0 & 4010 \end{bmatrix}\begin{pmatrix} h_1 \\ k_1 \\ l_1 \end{pmatrix} = \begin{pmatrix} h_2 \\ k_2 \\ l_2 \end{pmatrix} \quad (1)$$

transforms from primary to secondary Miller indices. The reverse operation is found by taking the inverse of the 3×3 matrix in Eq. (1).

The origin of this "hidden" domain can be understood as follows. As U atoms are deposited onto the Nb(110) surface, each nucleation event initiates the growth of a protodomain of α-U with a $\langle 110\rangle_U$ growth axis. In each of these newly forming protodomains, the atomic arrangements in the growth plane (i.e., the lowest layer in Fig. 6) can be considered identical. However, atoms in the subsequent monolayer have an energetically degenerate choice of bonding with the long bond on the left (and short bond on the right) or the reverse, creating either a left-skewed (B) or right-skewed (B′) layer. This choice fully constrains the growth axis and defines the domain. It is important to note that a 180° in-plane rotation fails to map one domain onto the other, instead stacking A/A′ directly above B/B′. The secondary domain origin must be shifted in-plane to ensure that the atomic sites are coincident in layer A.

If the growth mode is purely islandlike, the presence of these left- and right-skewed domains is likely to result in a columnar domain structure with in-plane antiphase domain boundaries. Pure layer-by-layer growth would preferentially create a layer with either left or right skewedness, as vertical switching of the "skewedness" would require the energetically unfavorable stacking of atoms almost directly above each other as shown in Fig. 6. The equal intensities of the two sets of reflections indicates equal domain occupations and the unlikelihood of direct atomic stacking suggests an islandlike or mixed-type growth mode, but a fully conclusive determination of the atomic stacking pattern across the domain boundaries

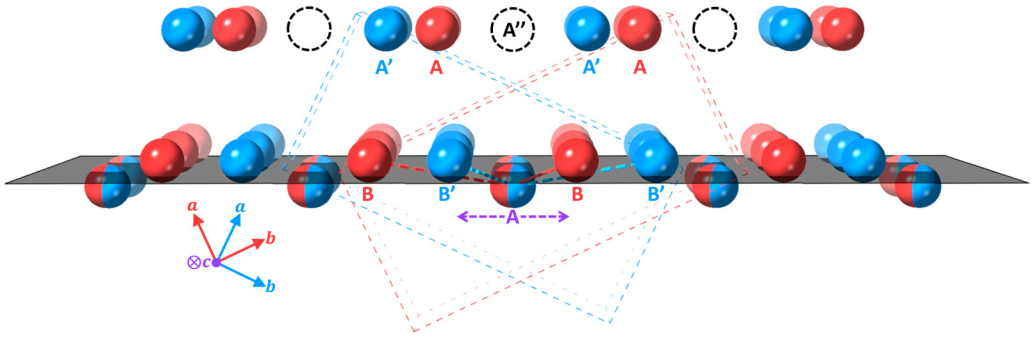

FIG. 6. Schematic representation of the crystallographic relationship between the two domains. Atoms are shown as colored spheres, unit cells by dashed cuboids, and axes by compass (bottom left). Colors are consistent with Fig. 5. The growth plane (translucent gray) corresponds to the (110) (primary) and $(1\bar{1}0)$ (secondary) planes. The first, degenerate, monolayer is marked with a purple label. The choice of atomic positions for the second monolayer is indicated by B/B′, with example bonds shown by dashed lines, and the resulting third monolayer positions by A/A′. The hypothetical atomic positions corresponding to the nonrotational domain switch are shown as dashed black circles and labeled A″.

requires the application of a nonaveraged technique, e.g., atomic resolution transmission electron microscopy.

It is important to acknowledge that this hidden domain should also be present in the Ti(00.1)/α-U(110) and Zr(00.1)/α-U(110) systems from previous sections. Indeed, these twin domains have been observed in (241) ϕ scans for both systems, but the scans have been omitted from this report due to their complexity. The true number of domains is then double the value suggested by the symmetry of the (221) ϕ scans.

IV. CONCLUSIONS

Several epitaxial α-U systems have been stabilized using both new (Ti, Zr) and known (Nb, W) elemental metallic buffer layers, with some U layers forming well-ordered systems without the need for substrate heating. The range of epitaxial strains and atomic volumes observed are expected to produce significant variations in the low temperature electronic properties. A combination of magnetotransport (e.g., Hall coefficient, resistivity, and magnetoresistance) and synchrotron diffraction measurements can now be used to probe the interplay between the CDW and SC ground states in these α-U thin films. Specifically, any superconducting states seen in the Ti, Zr and W buffered samples (where $T_c < 1$ K in the buffer) should be compared to those of high purity α-U single crystals ($T_c < 0.02$ K) [33], heavily disordered splat-cooled samples ($T_c \approx 1.2$ K) [34], and other crystals of intermediate quality [7–10] in order to disentangle the impact of strain and disorder on the superconductivity. Measurements of superconductivity in the Nb buffered systems will be more challenging ($T_c \approx 9.2$ K in bulk Nb), but T_c in the buffer could be suppressed by reducing its thickness or adding magnetic impurities. The complex structural information determined here will be essential for the accurate analysis and understanding of future electronic transport measurements conducted using α-U thin films.

ACKNOWLEDGMENTS

This research was supported by the Engineering and Physical Sciences Research Council (EPSRC), UK, through the Centre for Doctoral Training in Condensed Matter Physics (CDT-CMP), Grant No. EP/L015544/1, and the National Nuclear User Facility for Radioactive Materials Surfaces (NNUF-FaRMS), Grant No. EP/V035495/1 [35]. We also acknowledge the European Synchrotron Radiation Facility (ESRF) for provision of synchrotron radiation facilities.

[1] S. Elgazzar, J. Rusz, M. Amft, P. M. Oppeneer, and J. A. Mydosh, Hidden order in URu_2Si_2 originates from Fermi surface gapping induced by dynamic symmetry breaking, Nat. Mater. **8**, 337 (2009).

[2] I. M. Hayes, D. S. Wei, T. Metz, J. Zhang, Y. S. Eo, S. Ran, S. R. Saha, J. Collini, N. P. Butch, D. F. Agterberg, A. Kapitulnik, and J. Paglione, Multicomponent superconducting order parameter in UTe_2, Science **373**, 797 (2021).

[3] G. R. Stewart, Unconventional superconductivity, Adv. Phys. **66**, 75 (2017).

[4] R. Joynt and L. Taillefer, The superconducting phases of UPt_3, Rev. Mod. Phys. **74**, 235 (2002).

[5] D. L. Clark, D. A. Geeson, and R. Hanrahan, *Plutonium Handbook Vol. 6* (American Nuclear Society, La Grange Park, IL, 2019).

[6] K. T. Moore and G. van der Laan, Nature of the 5*f* states in actinide metals, Rev. Mod. Phys. **81**, 235 (2009).

[7] G. H. Lander, E. S. Fisher, and S. D. Bader, The solid-state properties of uranium A historical perspective and review, Adv. Phys. **43**, 1 (1994).

[8] R. D. Fowler, J. D. Lindsay, R. W. White, H. H. Hill, and B. T. Matthias, Positive isotope effect on the superconducting transition temperature of α-uranium, Phys. Rev. Lett. **19**, 892 (1967).

[9] J. L. O'Brien, A. R. Hamilton, R. G. Clark, C. H. Mielke, J. L. Smith, J. C. Cooley, D. G. Rickel, R. P. Starrett, D. J. Reilly, N. E. Lumpkin, R. J. Hanrahan, and W. L. Hults, Magnetic susceptibility of the normal-superconducting transition in high-purity single-crystal α-uranium, Phys. Rev. B **66**, 064523 (2002).

[10] G. M. Schmiedeshoff, D. Dulguerova, J. Quan, S. Touton, C. H. Mielke, A. D. Christianson, A. H. Lacerda, E. Palm, S. T. Hannahs, T. Murphy, E. C. Gay, C. C. McPheeters, D. J. Thoma, W. L. Hults, J. C. Cooley, A. M. Kelly, R. J. Hanrahan, and J. L. Smith, Magnetotransport and superconductivity of α-uranium, Philos. Mag. **84**, 2001 (2004).

[11] S. Raymond, J. Bouchet, G. H. Lander, M. Le Tacon, G. Garbarino, M. Hoesch, J. P. Rueff, M. Krisch, J. C. Lashley, R. K. Schulze, and R. C. Albers, Understanding the complex phase diagram of uranium: The role of electron-phonon coupling, Phys. Rev. Lett. **107**, 136401 (2011).

[12] R. Springell, R. C. C. Ward, J. Bouchet, J. Chivall, D. Wermeille, P. S. Normile, S. Langridge, S. W. Zochowski, and G. H. Lander, Malleability of uranium: Manipulating the charge-density wave in epitaxial films, Phys. Rev. B **89**, 245101 (2014).

[13] R. Springell, B. Detlefs, G. H. Lander, R. C. C. Ward, R. A. Cowley, N. Ling, W. Goetze, R. Ahuja, W. Luo, and B. Johansson, Elemental engineering: Epitaxial uranium thin films, Phys. Rev. B **78**, 193403 (2008).

[14] L. Xie, H. Yuan, and R. Qiu, Effect of strain on charge density wave order in α-U, Chin. Phys. B **31**, 067103 (2022).

[15] M. Yang, B. Ke, F. Zheng, T. Yi, Z. He, K. Du, L. Zhang, N. Li, L. Wang, and P. Xing, Microstructure and stability of the deposited beta-uranium films, J. Nucl. Mater. **547**, 152796 (2021).

[16] D. Chaney, A. Castellano, A. Bosak, J. Bouchet, F. Bottin, B. Dorado, L. Paolasini, S. Rennie, C. Bell, R. Springell, and G. H. Lander, Tuneable correlated disorder in alloys, Phys. Rev. Mater. **5**, 035004 (2021).

[17] S. Molodtsov, J. Boysen, M. Richter, P. Segovia, C. Laubschat, S. A. Gorovikov, A. M. Ionov, G. V. Prudnikova, and V. K. Adamchuk, Dispersion of $5f$ electron states: Angle-resolved photoemission on ordered films of U metal, Phys. Rev. B **57**, 13241 (1998).

[18] J. Boysen, P. Segovia, S. L. Molodtsov, W. Schneider, A. Ionov, M. Richter, and C. Laubschat, Dispersion of f states in U-metal and $CeRh_3$, J. Alloys Compd. **275-277**, 493 (1998).

[19] Q. Chen, S. Tan, W. Feng, L. Luo, X. Zhu, and X. Lai, Direct observation of the f-c hybridization in the ordered uranium films on W(110), Chin. Phys. B **28**, 077404 (2019).

[20] R. Springell, F. Wilhelm, A. Rogalev, W. G. Stirling, R. C. C. Ward, M. R. Wells, S. Langridge, S. W. Zochowski, and G. H. Lander, Polarization of U $5f$ states in uranium multilayers, Phys. Rev. B **77**, 064423 (2008).

[21] R. Nicholls, C. Bell, R. Springell, G. H. Lander, and J. Bouchet, Structure and phase transitions of metastable hexagonal uranium thin films, Phys. Rev. Mater. **6**, 103407 (2022).

[22] R. C. C. Ward, R. A. Cowley, N. Ling, W. Goetze, G. H. Lander, and W. G. Stirling, The structure of epitaxial layers of uranium, J. Phys.: Condens. Matter **20**, 135003 (2008).

[23] R. Springell, E. Lawrence Bright, D. A. Chaney, L. M. Harding, C. Bell, R. C. C. Ward, C. Bell, and G. H. Lander, A review of uranium-based thin films, Adv. Phys. 1 (2023).

[24] M. Björck and G. Andersson, GenX: An extensible x-ray reflectivity refinement program utilizing differential evolution, J. Appl. Crystallogr. **40**, 1174 (2007).

[25] A. Girard, T. Nguyen-Thanh, S. M. Souliou, M. Stekiel, W. Morgenroth, L. Paolasini, A. Minelli, D. Gambetti, B. Winkler, and A. Bosak, A new diffractometer for diffuse scattering studies on the ID28 beamline at the ESRF, J. Synchrotron Radiat. **26**, 272 (2019).

[26] Agilent Technologies, CrysAlisPro Data Collection and Processing Software for Agilent X-ray Diffractometers, 2014.

[27] DECTRIS, *ALBULA*, Tech. Rep., Philadelphia (unpublished).

[28] See Supplemental Material at http://link.aps.org/supplemental/10.1103/PhysRevMaterials.7.123602 for additional XRD/XRR data from the Ti/U and Zr/U systems.

[29] C. S. Barrett, M. H. Mueller, and R. L. Hitterman, Crystal structure variations in alpha uranium at low temperatures, Phys. Rev. **129**, 625 (1963).

[30] A. Gibaud, R. A. Cowley, D. F. McMorrow, R. C. C. Ward, and M. R. Wells, High-resolution x-ray-scattering study of the structure of niobium thin films on sapphire, Phys. Rev. B **48**, 14463 (1993).

[31] O. Durand, A. Letoublon, D. J. Rogers, and F. Hosseini Teherani, Interpretation of the two-components observed in high resolution x-ray diffraction ω scan peaks for mosaic ZnO thin films grown on c-sapphire substrates using pulsed laser deposition, Thin Solid Films **519**, 6369 (2011).

[32] A. G. Knapton, The crystal structure of TiU_2, Acta Crystallogr. **7**, 457 (1954).

[33] D. Graf, R. Stillwell, T. P. Murphy, J.-H. Park, M. Kano, E. C. Palm, P. Schlottmann, J. Bourg, K. N. Collar, J. C. Cooley, J. Lashley, J. Willit, and S. W. Tozer, Fermi surface of α-uranium at ambient pressure, Phys. Rev. B **80**, 241101(R) (2009).

[34] I. Tkach, N.-T. H. Kim-Ngan, A. Warren, T. Scott, and L. Havela, Electronic properties of γ-U and superconductivity of U-Mo alloys, Physica C: Superconductivity **498**, 14 (2014).

[35] https://nnuf-farms.bristol.ac.uk/.